

# Long-term evolution of orbits about a precessing\* oblate planet:

## 3. A semianalytical and a purely numerical approach.

Valéry Lainey

Observatoire Royal de Belgique, Avenue Circulaire 3, Bruxelles 1180 Belgium,  
 IMCCE/Observatoire de Paris, UMR 8028 du CNRS, 77 Avenue Denfert-Rochereau, Paris 75014 France  
 e-mail: Valery.Lainey @ imcce.fr ,

Pini Gurfil

Faculty of Aerospace Engineering, Technion, Haifa 32000 Israel  
 e-mail: pgurfil @ technion.ac.il ,

and

Michael Efroimsky

US Naval Observatory, Washington DC 20392 USA  
 e-mail: me @ usno.navy.mil

November 4, 2019

### Abstract

Construction of an accurate theory of orbits about a precessing and nutating oblate planet, in terms of osculating elements defined in a frame associated with the equator of date, was started in Efroimsky & Goldreich (2004) and Efroimsky (2005, 2006). Here we continue this line of research by combining that analytical machinery with numerics. The resulting semianalytical and seminumerical theory, based on the Lagrange-type planetary equations for the Keplerian elements, is then applied to Deimos on very long time scales (1 billion of years). In parallel with the said semianalytical theory for the Keplerian elements defined in the co-precessing equatorial frame, we have also carried out a completely independent, purely numerical, integration in a fixed inertial Cartesian frame. The results agree to within  $10^{-3} - 10^{-2}$  (from 0.3%, for near-polar orbits, through 1.3% for near-equatorial ones), for over 20 Myr, thus demonstrating the applicability of our semianalytical model over long timescales. This will enable us to employ the semianalytical model at the further stages of the project, enriching this model with the tides, the gravitational pull of the Sun, and the planet's triaxiality. (Efroimsky, Gurfil & Lainey 2007)

---

\* We use the term “precession” in its general meaning, which includes any change of the instantaneous spin axis. So generally defined precession embraces the entire spectrum of spin-axis variations – from the polar wander and nutations through the Chandler wobble through the equinoctial precession.

Another goal of this work was to make an independent check of whether the equinoctial precession of Mars, as predicted for a rigid Mars, could have been sufficient to repel the orbits away from the equator. The answer to this question, in combination with our knowledge of the current position of Phobos and Deimos, will help us to understand whether this precession could indeed have always been as large as predicted or whether it ought to have been less in the past. It has turned out that, both for high and low initial inclinations, the orbit inclination, reckoned from the precessing equator of date, is subject only to small variations (from about  $10^{-3}$  deg, for near-equatorial satellites, to about 2 deg, for polar ones). This is an extension, to non-uniform equinoctial precession given by the Colombo model and to an arbitrary initial inclination, of an old result obtained by Goldreich (1965) for the case of uniform precession and a low initial inclination. Such “inclination locking,” or the “Goldreich lock,” confirms that an oblate planet can, indeed, afford a large equinoctial precession for billions of years, without repelling its near-equatorial satellites away from the equator of date: the satellite inclination oscillates but does not show a secular increase. Nor does it show a secular decrease, a fact that is relevant to the discussion of the possibility of high-inclination capture of Phobos and Deimos.

# 1 Introduction

## 1.1 Statement of purpose

The goal of this paper is to explore, by two very different methods, inclination variations of a satellite orbiting an oblate planet subject to nonuniform equinoctial precession. This nonuniformity of precession is caused by the presence of the other planets. Their gravitational pull entails precession of the circumsolar orbit of our planet; this entails variations of the solar torque acting on it; these torque variations make the planet’s equinoctial precession nonuniform; and this nonuniformity, in its turn, influences the behaviour of the planet’s satellites. This influence is feeble, and we trace with a great accuracy whether over huge spans of time it results in purely periodic changes in inclination or can accumulate to secular changes.

It should be emphasised that this work is but a small part of a larger project, the eventual goal whereof will be to build up a comprehensive tool for computation of long-term orbital evolution of satellites. The tool, in its final form, will contain the triaxiality, the tides, the influence of the Sun upon the satellite’s motion, and the planet’s precession. Building this tool, block by block, we are beginning with the primary’s precession, phenomenon that bares a marked effect on the evolution of the orbit. In our subsequent publications, we shall incorporate more effects into our model –  $J_2^2$ , the triaxiality, the tides, and the pull of the Sun on the satellite.

## 1.2 Motivation

One motivation for this work stems from our intention to carry out an independent check of whether Mars could have performed, through all of its past history, the same large equinoctial precession as it is performing at present. Such a check is desirable because the current theory of equinoctial precession, based on the Colombo model, incorporates, as any theory, certain approximations. First, the Colombo equation is derived under the assertion that the planet is rigid and that it is always in its principal spin state, the angular-momentum vector staying parallel to the angular-velocity one. Second, this description, being only a model, ignores the possibility of planetary catastrophes that might have altered the planet’s spin mode. Fortunately, in the case of Mars there may exist a model-independent test that may bring restrictions on the amplitude

of the equinoctial precession in the past. This test is based on the necessity to reconcile the variations of spin with the present near-equatorial positions of Phobos and Deimos. The fact that both moons found themselves on near-equatorial orbits, in all likelihood, billions of years ago,<sup>1</sup> and that both are currently located within less than  $2^\circ$  degrees from the equator, is surely more than a mere coincidence. An elegant but sketchy calculation by Goldreich (1965) demonstrated that the orbits of initially near-equatorial satellites remain close to the equator of date for as long as some simplifying assumptions remain valid. As explained by Efroimsky (2005), these assumptions are valid over time scales not exceeding 100 million years, while at longer times a more careful analysis is required. Its goal will be to explore the limits for the possible secular drift of the satellite orbits away from the evolving equator of date. Through comparison of these limits with the present location of the Martian satellites, we shall be able to impose restrictions upon the long-term spin variations of Mars. If, however, it turns out that near-equatorial satellites can, in the face of large equinoctial precession of the oblate primary, remain for billions of years close to the moving equator of date, then we shall admit that Mars' equator is likely to have precessed through billions of years in the same manner as it is doing now.

The second motivation for our study comes from the ongoing discussion of whether the Martian satellites might have been captured at high inclinations, their orbits having gradually approached the equator afterwards. While a comprehensive check of this hypothesis will need a more detailed model – one that will include Mars' triaxiality, the Sun, the tidal forces, (Efroimsky, Gurfil, & Lainey 2007), and perhaps even relativistic corrections – the first, rough sketch of this test can be carried out with only  $J_2$  and the equinoctial precession taken into account. We perform such a rough check for a hypothetical satellite that has all the parameters of Deimos, except that its initial inclination is  $89^\circ$ .

### 1.3 Mathematical tools

The first steps toward the analytical theory of orbits about a precessing and nutating Earth were undertaken almost half a century ago by Brouwer (1959), Proskurin & Batrakov (1960), and Kozai (1960). This problem was considered, in application to the Martian satellites, by Goldreich (1965) and, in regard to a circumlunar orbiter, by Brumberg, Evdokimova, & Kochina (1971). The latter two publications addressed the dynamics as seen in a non-inertial frame associated with the planet's equator of date. The analysis was carried out in terms of the so-called “contact” Kepler elements, i.e., in terms of the Kepler elements satisfying a condition different from that of osculation. Modelling of perturbed trajectories by sequences of instantaneous ellipses (or hyperbolae) parameterised with such elements is sometimes very convenient mathematically (Efroimsky 2002a,b; Newman & Efroimsky 2003; Efroimsky & Goldreich 2003, 2004). However,

---

<sup>1</sup> Phobos and Deimos give every appearance of being captured asteroids of the carbonaceous chondritic type, with cratered surfaces older than  $\sim 10^9$  years (Veverka 1977; Pang et al. 1978; Pollack et al. 1979; Tolson et al. 1978). If they were captured by gas drag (Burns 1978), this must have occurred early in the history of the solar system while the gas disk was substantial enough. At that stage of planetary formation, the spin of the forming planet would be perpendicular to the planet's orbit about the Sun – i.e., the obliquity would be small and the gas disk would be nearly coplanar with the planetary orbit. Energetically, a capture would likely be equatorial. This is most easily seen in the context of the restricted three-body problem. The surfaces of zero velocity constrain any reasonable capture to occur from directions near the inner and outer collinear Lagrange points (Szebehely 1967, Murison 1988), which lie in the equatorial plane. Also, a somewhat inclined capture would quickly be equatorialised by the gas disk. If the capture inclination is too high, the orbital energy is then too high to allow a long enough temporary capture, and the object would hence not encounter enough drag over a long enough time to effect a permanent capture (Murison 1988). Thus, Phobos and Deimos were likely (in as much as we can even use that term) to have been captured into near-equatorial orbits.

the physical interpretation of such solutions is problematic, because instantaneous conics defined by nonosculating elements are nontangent to the trajectory. Though over restricted time scales the secular parts of the contact elements may well approximate the secular parts of their osculating counterparts (Efroimsky 2005), the cleavage between them may grow at longer time scales (Efroimsky 2006). This is the reason wherefore a practically applicable treatment of the problem must be performed in the language of osculating variables.

## 1.4 The plan

The analytical theory of orbits about a precessing oblate primary, in terms of the Kepler elements defined in a co-precessing (i.e., related to the equator of date) frame, was formulated in Efroimsky (2006) where the planetary equations were approximated through averaging some of their terms. This way, from the exact equations for osculating elements, approximate equations for their secular parts were obtained. We shall borrow those averaged Lagrange-type planetary equations and shall numerically explore their solutions. This will give us a method that will be semianalytical and seminumerical. We shall then apply it to a particular setting – evolution of a Martian satellite and its reaction to the long-term variations of the spin state of Mars. Our goal will be to explore whether the spin-axis variations predicted for a rigid Mars permit its satellites to remain close to the equator of date for hundreds of millions through billions of years. In case the answer to this question turns out to be negative, it will compel us to seek nonrigidity-caused restrictions upon the spin variations. Otherwise, the calculations of the rigid-Mars inclination variations will remain in force (and so will the subsequent calculations of Mars obliquity variations); this way, the theory of Ward (1973, 1974, 1979, 1982) will get a model-independent confirmation.

## 2 Semianalytical treatment of the problem

To understand the evolution of a satellite orbit about a precessing planet, it is natural to model it with elements defined in a coordinate system associated with the equator of date, i.e., in a frame co-precessing (but not co-rotating) with the planet. A transition from an inertial frame to the co-precessing one is a perturbation that depends not only upon the instantaneous position but also upon the instantaneous velocity of the satellite. It has been demonstrated by Efroimsky & Goldreich (2004) that such perturbations enter the planetary equations in a nontrivial way: not only they alter the disturbing function (which is the negative Hamiltonian perturbation) but also they endow the equations with several extra terms that are not parts of the disturbing function. Some of these nontrivial terms are linear in the planet's precession rate  $\vec{\mu}$ , some are quadratic in it; the rest are linear in its time derivative  $\dot{\vec{\mu}}$ . The inertial-forces-caused addition to the disturbing function (i.e., to the negative Hamiltonian perturbation) consists of a term linear and a term quadratic in  $\vec{\mu}$ . (See formulae (1) and (6) in Efroimsky (2006) or formulae (53 - 54) in Efroimsky (2005).) The essence of approximation elaborated in Efroimsky (2006) was to neglect the quadratic terms and to substitute the terms linear in  $\vec{\mu}$  and  $\dot{\vec{\mu}}$  with their secular parts calculated with precision up to  $e^3$ , inclusively.

## 2.1 Equations for the secular parts of osculating elements defined in a co-precessing reference frame.

We shall begin with five Lagrange-type planetary equations for the secular parts of the orbital elements, derived in Efroimsky (2005):

$$\frac{da}{dt} = -2 \frac{\dot{\mu}_\perp}{n} a (1 - e^2)^{1/2} , \quad (1)$$

$$\frac{de}{dt} = \frac{5}{2} \frac{\dot{\mu}_\perp}{n} e (1 - e^2)^{1/2} , \quad (2)$$

$$\frac{d\omega}{dt} = \frac{3}{2} \frac{n J_2}{(1 - e^2)^2} \left( \frac{\rho_e}{a} \right)^2 \left( \frac{5}{2} \cos^2 i - \frac{1}{2} \right) - \mu_\perp + \mu_n \cot i - \frac{\cos i}{na^2(1 - e^2)^{1/2} \sin i} \langle \dot{\vec{\mu}} \left( -\vec{f} \times \frac{\partial \vec{f}}{\partial i} \right) \rangle , \quad (3)$$

$$\begin{aligned} \frac{di}{dt} &= -\mu_1 \cos \Omega - \mu_2 \sin \Omega \\ &+ \frac{\cos i}{na^2(1 - e^2)^{1/2} \sin i} \langle \dot{\vec{\mu}} \left( -\vec{f} \times \frac{\partial \vec{f}}{\partial \omega} \right) \rangle - \frac{1}{na^2(1 - e^2)^{1/2} \sin i} \langle \dot{\vec{\mu}} \left( -\vec{f} \times \frac{\partial \vec{f}}{\partial \Omega} \right) \rangle , \end{aligned} \quad (4)$$

$$\frac{d\Omega}{dt} = -\frac{3}{2} n J_2 \left( \frac{\rho_e}{a} \right)^2 \frac{\cos i}{(1 - e^2)^2} - \frac{\mu_n}{\sin i} + \frac{1}{na^2(1 - e^2)^{1/2} \sin i} \langle \dot{\vec{\mu}} \left( -\vec{f} \times \frac{\partial \vec{f}}{\partial i} \right) \rangle , \quad (5)$$

The number of equations is five, because one element,  $M_o$ , was excluded by averaging of the Hamiltonian perturbation and of the inertial terms emerging in the right-hand sides. In the equations,  $n \equiv \sqrt{G(m_{primary} + m_{secondary})/a^3}$ , while  $\vec{f}(t; a, e, i, \omega, \Omega, M_o)$  is the implicit function that expresses the unperturbed two-body dependence of the position upon the time and Keplerian elements. Vector  $\vec{\mu}$  denotes the total precession rate of the planetary equator (including all spin variations – from the polar wander and nutations through the Chandler wobble through the equinoctial precession through the longest-scale spin variations caused by the other planets' pull), while  $\mu_1, \mu_2, \mu_3$  stand for the components of  $\vec{\mu}$  in a co-precessing coordinate system  $x, y, z$ , the axes  $x$  and  $y$  belonging to the equator-of-date plane, and the longitude of the node,  $\Omega$ , being measured from  $x$ :

$$\vec{\mu} = \mu_1 \hat{\mathbf{x}} + \mu_2 \hat{\mathbf{y}} + \mu_3 \hat{\mathbf{z}} , \quad \text{where} \quad \mu_1 = \dot{I}_p , \quad \mu_2 = \dot{h}_p \sin I_p , \quad \mu_3 = \dot{h}_p \cos I_p , \quad (6)$$

$I_p, h_p$  being the inclination and the longitude of the node of the equator of date relative to that of epoch, and dot standing for a time derivative. The quantity  $\mu_\perp$  is a component of  $\vec{\mu}$  directed along the instantaneous orbital momentum of the satellite, i.e., perpendicular to the instantaneous osculating Keplerian ellipse. This component will be expressed with

$$\mu_\perp \equiv \vec{\mu} \cdot \vec{w} = \mu_1 \sin i \sin \Omega - \mu_2 \sin i \cos \Omega + \mu_3 \cos i , \quad (7)$$

the unit vector

$$\vec{w} = \hat{\mathbf{x}} \sin i \sin \Omega - \hat{\mathbf{y}} \sin i \cos \Omega + \hat{\mathbf{z}} \cos i \quad (8)$$

standing for the normal to the instantaneous osculating ellipse. Be mindful that the quantity  $\dot{\mu}_\perp$  is defined not as  $d(\vec{\mu} \cdot \vec{w})/dt$  but as

$$\dot{\mu}_\perp \equiv \dot{\vec{\mu}} \cdot \vec{w} = \dot{\mu}_1 \sin i \sin \Omega - \dot{\mu}_2 \sin i \cos \Omega + \dot{\mu}_3 \cos i \quad . \quad (9)$$

The quantity  $\mu_n$  is a component pointing toward the ascending node of the satellite orbit relative to the equator of date:

$$\begin{aligned} \mu_n &= -\mu_1 \sin \Omega \cos i + \mu_2 \cos \Omega \cos i + \mu_3 \sin i \\ &= -\dot{I}_p \sin \Omega \cos i + \dot{h}_p \sin I_p \cos \Omega \cos i + \dot{h}_p \cos I_p \sin i \quad . \end{aligned} \quad (10)$$

Its time derivative taken in the frame of reference co-precessing with the equator of date is:

$$\begin{aligned} \dot{\mu}_n &= -\dot{\mu}_1 \sin \Omega \cos i + \dot{\mu}_2 \cos \Omega \cos i + \dot{\mu}_3 \sin i \\ &= -\ddot{I}_p \sin \Omega \cos i + \left( \ddot{h}_p \sin I_p + \dot{h}_p \dot{I}_p \cos I_p \right) \cos \Omega \cos i + \left( \ddot{h}_p \cos I_p - \dot{h}_p \dot{I}_p \sin I_p \right) \sin i \quad . \end{aligned} \quad (11)$$

As shown in Efroimsky (2006), the  $\dot{\vec{\mu}}$ -dependent terms, emerging in equations (1 - 5), are expressed with

$$\begin{aligned} \langle \dot{\vec{\mu}} \cdot \left( -\vec{f} \times \frac{\partial \vec{f}}{\partial i} \right) \rangle &= \\ \frac{a^2}{4} \left\{ \dot{\mu}_1 \left[ - (2 + 3e^2) \cos \Omega + 5e^2 (\cos \Omega \cos 2\omega - \sin \Omega \sin 2\omega \cos i) \right] + \right. \\ \dot{\mu}_2 \left[ - (2 + 3e^2) \sin \Omega + 5e^2 (\sin \Omega \cos 2\omega + \cos \Omega \sin 2\omega \cos i) \right] + \\ \left. \dot{\mu}_3 \left[ 5e^2 \sin 2\omega \sin i \right] \right\} \end{aligned} \quad (12)$$

$$\langle \dot{\vec{\mu}} \cdot \left( -\vec{f} \times \frac{\partial \vec{f}}{\partial \omega} \right) \rangle = -\frac{a^2}{2} (2 + 3e^2) (\dot{\mu}_1 \sin i \sin \Omega - \dot{\mu}_2 \sin i \cos \Omega + \dot{\mu}_3 \cos i) \quad , \quad (13)$$

$$\begin{aligned}
\langle \dot{\vec{\mu}} \cdot \left( -\vec{f} \times \frac{\partial \vec{f}}{\partial \Omega} \right) \rangle = \\
\frac{a^2}{4} \left\{ \dot{\mu}_1 \sin i \left[ - (2 + 3e^2) \sin \Omega \cos i + 5e^2 (\cos \Omega \sin 2\omega + \sin \Omega \cos 2\omega \cos i) \right] \right. \\
+ \dot{\mu}_2 \sin i \left[ (2 + 3e^2) \cos \Omega \cos i + 5e^2 (\sin \Omega \sin 2\omega - \cos \Omega \cos 2\omega \cos i) \right] \\
\left. - \dot{\mu}_3 \left[ (2 + 3e^2) (2 - \sin^2 i) + 5e^2 \sin^2 i \cos 2\omega \right] \right\} \quad (14)
\end{aligned}$$

To integrate equations (1 - 5), with expressions (12 - 14) inserted therein, we shall need to know, at each step of integration, the components of  $\vec{\mu}$  and  $\dot{\vec{\mu}}$ .

## 2.2 Calculation of the components of $\vec{\mu}$ and $\dot{\vec{\mu}}$ .

At each step of our integration, the components of  $\vec{\mu}$  and  $\dot{\vec{\mu}}$  will be calculated in the Colombo approximation. Physically, the essence of this approximation is two-fold: first, the solar torque acting on the planet is replaced by its average over the year; and, second, the precessing planet is assumed to be always in its principal spin state. While a detailed development (based on the work by Colombo (1966)) may be found in the Appendix to Efroimsky (2006), here we shall provide a concise list of resulting formulae to be used.

The components of  $\vec{\mu}$  are connected, through the medium of (6), with the inclination and the longitude of the node of the moving planetary equator,  $I_p$  and  $h_p$ , relative to some equator of epoch. These quantities and their time derivatives are connected with the unit vector  $\hat{\mathbf{k}}$  aimed in the direction of the major-inertia axis of the planet:

$$\hat{\mathbf{k}} = (\sin I_p \sin h_p, -\sin I_p \cos h_p, \cos I_p)^T. \quad (15)$$

This unit vector and its time derivative

$$\frac{d\hat{\mathbf{k}}}{dt} = \left( \dot{I}_p \cos I_p \sin h_p + \dot{h}_p \sin I_p \cos h_p, -\dot{I}_p \cos I_p \cos h_p + \dot{h}_p \sin I_p \sin h_p, -\dot{I}_p \sin I_p \right)^T, \quad (16)$$

depend, through the Colombo equation

$$\frac{d\hat{\mathbf{k}}}{dt} = \alpha (\hat{\mathbf{n}} \cdot \hat{\mathbf{k}}) (\hat{\mathbf{k}} \times \hat{\mathbf{n}}), \quad (17)$$

upon the unit normal to the planetary orbit,

$$\hat{\mathbf{n}} = (\sin I_{orb} \sin \Omega_{orb}, -\sin I_{orb} \cos \Omega_{orb}, \cos I_{orb})^T, \quad (18)$$

$h_{orb}$  and  $I_{orb}$  being the node and inclination of the orbit relative to some fiducial fixed plane.

Hence, to find the components of  $\vec{\mu}$ , one must know the time evolution of  $h_p$  and  $I_p$ , which can be determined by solving a system of three differential equations (17), with  $h_{orb}$  and  $I_{orb}$  being some known functions of time. These functions may be computed via the auxiliary variables

$$q = \sin I_{orb} \sin \Omega_{orb} , \quad p = \sin I_{orb} \cos \Omega_{orb} , \quad (19)$$

whose evolution will be given by the formulae of Brouwer & van Woerkom (1950):

$$q = \sum_{j=1}^{\infty} N_j \sin (s'_j t + \delta_j) , \quad (20)$$

$$p = \sum_{j=1}^{\infty} N_j \cos (s'_j t + \delta_j) . \quad (21)$$

The following choice of the values of the amplitudes, frequencies, and phases will make equations (19 - 21) render  $h_{orb}$  and  $I_{orb}$  relative to the ecliptic plane of 1950:<sup>2</sup>

$j$	$N_j$	$s'_j$ (arc sec/yr)	$\delta'_j$ (deg)
1	0.0084889	- 5.201537	19.43255
2	0.0080958	- 6.570802	318.05685
3	0.0244823	- 18.743586	255.03057
4	0.0045254	- 17.633305	296.54103
5	0.0275703	+ 0.000004	107.10201
6	0.0028112	- 25.733549	127.36669
7	- 0.0017308	- 2.902663	315.06348
8	- 0.0012969	- 0.677522	202.29272

The development by Brouwer & van Woerkom (1950) is limited in precision and, therefore, in the time span over which it remains valid. A far more accurate and comprehensive development, which remains valid for (at least) tens of millions of years, was offered by Laskar (1988). At the future stages of our project, when developing a detailed physical model of the satellite motion, we shall employ Laskar's results. At this point we can save computer time by using the simple old formalism by Brouwer and van Woerkom, because our present goal is restricted: in the current paper, we are not yet building a consistent physical model, but are simply checking if the orbital averaging of the precession-caused terms is permissible at large time scales. Hence, for the purpose of this check we need a realistic, not necessarily real, scenario of the precession variations.

<sup>2</sup> This plane may well be chosen as fiducial, because one may assume without loss of generality that at some initial, very distant, instant of time the satellite orbit belonged to that plane.

## 2.3 The Goldreich approximation

The above semianalytical treatment not only yields plots of the time dependence of the mean elements but also serves as a launching pad for analytical approximations. For example, an assumption of  $a$  and  $e$  being constant, and a neglect of the  $\vec{\mu}$ -dependent terms in (4 - 5), as well as of the term  $\mu_n / \sin i$  in (5), gives birth to the Goldreich (1965) approximation:

$$\frac{da}{dt} = 0 , \quad (22)$$

$$\frac{de}{dt} = 0 , \quad (23)$$

$$\frac{di}{dt} = -\mu_1 \cos \Omega - \mu_2 \sin \Omega , \quad (24)$$

$$\frac{d\Omega}{dt} = -\frac{3}{2} n J_2 \left(\frac{\rho_e}{a}\right)^2 \frac{\cos i}{(1-e^2)^2} , \quad (25)$$

$$\frac{d\omega}{dt} = \frac{3}{4} n J_2 \left(\frac{\rho_e}{a}\right)^2 \frac{5 \cos^2 i - 1}{(1-e^2)^2} + \frac{\mu_n}{\cos i \sin i} - \mu_\perp , \quad (26)$$

the equinoctial precession being assumed uniform:

$$\dot{I}_p = 0 \quad (27)$$

$$\dot{h}_p = \alpha \quad (28)$$

$$\mu_1 = 0 \quad (29)$$

$$\mu_2 = 0 \quad (30)$$

$$\mu_3 = \dot{h}_p \cos I_p . \quad (31)$$

For the details of Goldreich's approximation see also subsection 3.3 in Efroimsky (2005).

## 3 A purely numerical treatment of the problem

Our main goal is to check the applicability limits (both in terms of the initial conditions and the permissible time scales) of our approximate system (1 - 5) written for the osculating elements introduced in a frame co-precessing with the equator of date. This check will be performed by an independent straightforward, purely numerical, computation that will be free from whatever simplifying assumptions. The check will be carried out in terms of Cartesian coordinates and velocities defined in an inertial frame of reference. Both the semianalytical calculation of the elements in a coprecessing frame and the straightforward numerical integration in inertial Cartesian axes will be carried out for Deimos.

### 3.1 The numerical algorithm, the units, the constants, and the initial conditions.

The numerical integration of Deimos' orbit can be performed using Cartesian coordinates in the J1950 inertial reference frame. As we also have to compute the Martian polar axis motion, there are two vector differential equations to integrate simultaneously. One is the Newton gravity law:

$$\ddot{\vec{r}} = -\frac{G (M + m) \vec{r}}{r^3} + G (M + m) \nabla U , \quad (32)$$

where  $\nabla U$  has components

$$\left\{ \begin{array}{l} \partial_x U = \frac{\rho_e^2 J_2}{r^4} \left[ \frac{x}{r} \left( \frac{15}{2} \sin^2 \phi - \frac{3}{2} \right) - 3 \sin \phi \sin I_p \sin h_p \right] \\ \partial_y U = \frac{\rho_e^2 J_2}{r^4} \left[ \frac{y}{r} \left( \frac{15}{2} \sin^2 \phi - \frac{3}{2} \right) + 3 \sin \phi \sin I_p \cos h_p \right] \\ \partial_z U = \frac{\rho_e^2 J_2}{r^4} \left[ \frac{z}{r} \left( \frac{15}{2} \sin^2 \phi - \frac{3}{2} \right) - 3 \sin \phi \cos I_p \right] \end{array} \right. . \quad (33)$$

Here  $\phi$  and  $\vec{r} = (x, y, z)$  denote, correspondingly, the latitude of Deimos relative to the Martian equator and the position vector of Deimos related to the Martian center of mass;  $\rho_e$  is the Martian equatorial radius;  $M$  and  $m$  stand for the masses of Mars and Deimos, respectively. Angles  $h_p$  and  $I_p$  are the longitude of the node and the inclination of the planet's equator of date relative to that of epoch. Without loss of generality, we identify the equator of epoch with the  $XY$  plane of the J1950 coordinate system. This enables us to assume that the above equation (33) is written down in this system. Integration in this, inertial, frame offers the obvious advantage of nullifying the inertial forces.

Table 1 gives the initial conditions for our simulation, expressed in terms of the Keplerian orbital elements. Table 2 presents these initial conditions in a more practical form, i.e., in terms of the Cartesian positions and velocities corresponding to the said elements. A transition from the Keplerian elements to these Cartesian positions and velocities is a two-step process. First, we take orbital elements defined in a frame associated with the Martian equator of date (i.e., in a frame coprecessing but not corotating with the planet) and transform them into Cartesian coordinates and velocities defined in that same frame. Then, by two successive rotations of angles  $-I_p$  and  $-h_p$ , we transform them into Cartesian coordinates and velocities related to the J1950 reference frame. These initial positions and velocities were used to begin the integration.

At each step of integration of (32), the same two rotations are performed on the components  $\nabla U$  given by (33). As mentioned above, to afford the absence of inertial forces on the right-hand side of (32) one must write down and integrate (32) in the inertial J1950 frame. Since the analytical expressions (33) for  $\nabla U$  contain the latitude  $\phi$ , they are valid in the coprecessing coordinate system and, therefore, need to be transformed to J1950 at each step. To carry out the transformation, one needs to know, at each step, the relative orientation of the Martian polar axis and the inertial J1950 coordinate system. The orientation is given by the afore mentioned Colombo model. This is how our second equation, the one of Colombo, comes into play:

$$\frac{d\mathbf{k}}{dt} = \alpha(\hat{\mathbf{k}} \cdot \hat{\mathbf{n}})(\hat{\mathbf{k}} \times \hat{\mathbf{n}}) . \quad (34)$$

All in all, we have to integrate the system (32 - 34). Table 3 gives the initial conditions used for integrating (34), while Table 4 gives the numerical values used for the parameters involved.

The software used for numerical integration of the system (32 - 34) is called NOE (Numerical Orbit and Ephemerides), and is largely based on the ideas and methods developed in Lainey, Duriez & Vienne (2004). This numerical tool was created at the Royal Observatory of Belgium mainly for computations of the natural satellite ephemerides. It is an  $N$ -body code, which incorporates highly sensitive modelling and can generate partial derivatives. The latter are needed when one wants to fit the initial positions, velocities, and other parameters to the observation data. To save the computer time, an optimised force subroutine was built into the code, specifically for integrating the above equations. This appliance, based on the RA15 integrator offered

by Everhart (1985), was chosen for its speed and accuracy. During the integration, a variable step size with an initial value of 0.04 day was used. To control the numerical error, back and forth integrations were performed. In particular, we carried out a trial simulation consisting of a thousand-year forward and a subsequent thousand-year back integration. The satellite displacement due to the error accumulated through this trial was constrained to 150 meters. Most of this 150 meter difference comes from a numerical drift of the longitude, while the numerical errors in the computation of the semi-major axis, the eccentricity, and the inclination were much lower. These errors were reduced for this trial simulation to only  $10^{-5}$  km,  $10^{-10}$ , and  $10^{-10}$  degree, respectively. This provided us with a high confidence in our subsequent numerical results.

As a complement to the said back-and-forth check, the energy-conservation criterium was used to deduce, in the first approximation, an optimal initial step-size value and to figure out the numerical error proliferation. (It is for this energy-conservation test that we introduced a non-zero mass for Deimos. Its value was taken from Smith, Lemoine & Zuber (1995).) Applicability of this criterium is justified by the fact that the numerical errors are induced mostly by the fast orbital motion of the satellite.<sup>3</sup>

parameters	numerical values
$a$	23459 km
$e$	0.0005
$i$	0.5 deg. and 89 deg.
$\Omega$	10 deg.
$\omega$	5 deg.
$M$	0 deg.

Table 1: The orbital elements' values taken as initial conditions for our simulations.

satellite	$x$	$y$	$z$
position km ( $i = 0.5$ )	23358.6525447458	2040.90967963532	-35.9715582515763
velocity $km s^{-1}$ ( $i = 0.5$ )	-0.117066266533499	1.34018324055820	0.133068449913892
position km ( $i = 89$ )	22291.4778850948	6256.65104491350	-3706.42501342002
velocity $km s^{-1}$ ( $i = 89$ )	0.231350273413379	$-3.619316279591354 \times 10^{-2}$	1.33141651910815

Table 2: The initial positions and velocities used for Deimos, in the Earth equatorial J1950 frame centered on Mars. The first two rows correspond to the low-inclination case (0.5 degree); the last two rows correspond to the high-inclination case (89 degrees).

---

<sup>3</sup>Although the planet-satellite system is subject to an external influence (the solar torque acting on the planet), over short time scales this system can be assumed closed. In order to check the integrator efficiency and to determine an optimal initial step size, we carried out auxiliary integrations of (32) - (33), with the Colombo equation (34) neglected and with the energy presumed to conserve. These several-thousand-year-long trial integrations, with the energy-conservation criterium applied, led us to the conclusion that our integrator remained steady over long time scales and that the initial step of 0.04 day was optimal. Then this initial step size was employed in our integration of the full system (32) - (34).

parameters	numerical values
$I_p(t_0)$	5.156620156177409 deg.
$h_p(t_0)$	5 deg.

Table 3: Initial conditions used for the integration of equation (34).

parameters	numerical values
Martian mass (GM)	$42830 \text{ km}^3 \text{s}^{-2}$
$J_2$	$1960.45 \times 10^{-6}$
Equatorial radius	3397 km
Deimos mass	$0.091 \times 10^{-3} \text{ km}^3 \text{s}^{-2}$
$\alpha$	$3.9735 \times 10^{-5} \text{ rad/yr}$

Table 4: Parameters' values used in our simulations.

### 3.2 The results of the straightforward integration.

The theory of satellite-orbit evolution, based on the planetary equations (1 - 5), is semianalytical. This means that these equations for the elements' secular parts are derived analytically, but their integration is to be performed numerically. This integration was carried out using an 8th-order Runge-Kutta scheme with relative and absolute tolerances of  $10^{-12}$ . Kilograms, years, and kilometers were taken as the mass, time, and length units, correspondingly.

#### 3.2.1 Technicalities

To integrate the planetary equations (1 - 5), one should know, at each time step, the values of  $\dot{I}_p$  and  $\dot{h}_p$ , which are the time derivatives of the inclination and of the longitude of the node of the equator of date with respect to the equator of epoch. These derivatives will be rendered by the Colombo equation (17), after formulae (15 - 16) get inserted therein:

$$\begin{aligned} \dot{I}_p = & -\alpha \left( q^2 \sin I_p \sin h_p \cos h_p - q p \sin I_p + 2 p q \sin I_p \cos^2 h_p \right. \\ & - p^2 \sin I_p \cos h_p \sin h_p + q \sqrt{1 - q^2 - p^2} \cos I_p \cos h_p \\ & \left. - p \sqrt{1 - q^2 - p^2} \cos I_p \sin h_p \right) , \end{aligned} \quad (35)$$

and

$$\begin{aligned} \dot{h}_p = & -\alpha \left\{ \left[ (p - 2p \cos^2 I_p) \cos h_p + \frac{(-q + 2q \cos^2 I_p) \cos^2 h_p - 2q \cos^2 I_p + q}{\sin h_p} \right] \frac{\sqrt{1 - p^2 - q^2}}{\sin I_p} \right. \\ & + (q^2 - p^2) \cos I_p \cos^2 h_p + (-p^2 - 2q^2 + 1) \cos I_p \\ & \left. + \frac{2qp \cos I_p \cos^3 h_p - 2pq \cos h_p \cos I_p}{\sin h_p} \right\} . \end{aligned} \quad (36)$$

Equations (35) and (36) are then integrated (with the initial conditions  $I_p(t_0)$  and  $h_p(t_0)$  borrowed from Table 3) simultaneously with the planetary equations (1 - 5). Through formulae (6), the above expressions for  $I_p$  and  $h_p$  yield the expressions for the components of  $\vec{\mu}$ . As can be seen from (12 - 14), integration of (1 - 5) also requires the knowledge of the derivatives  $\dot{\mu}_1$ ,  $\dot{\mu}_2$ , and  $\dot{\mu}_3$  at each integration step. These can be readily obtained by differentiating (6). The resulting closed-formed expressions for  $\dot{\mu}_1$ ,  $\dot{\mu}_2$ ,  $\dot{\mu}_3$  are listed in Appendix A. The final step required for numerical integration of equations (1) - (5) is substitution of formulae (9 - 12), with the initial conditions from Table 1.

### 3.2.2 The plots and their interpretation

Fig. 1 depicts the history of the planetary equator, in the Colombo approximation, over 1 Bln years. The inclination exhibits long-periodic oscillations bounded within the range of  $1.8 \text{ deg} \leq I_p \leq 12.3 \text{ deg}$ , while the node regresses at a rate of  $\dot{h}_p = 0.00225 \text{ deg/yr}$ .

Suppose that at the initial instant of time a satellite was close to the equator of date:  $i_0 = 0.5 \text{ deg}$ . Integration of our semianalytical model gives plots depicted in Figures 2 and 3, for a low initial inclination, and in Figures 4 and 5, for a high initial inclination. From Fig. 2 we see that the variable equinoctial precession does not inflict considerable changes on the satellite's inclination on the precessing equator of date: the orbit inclination remains bounded within the region  $0.493 \text{ deg} \leq i \leq 0.502 \text{ deg}$ . This means that the "Goldreich lock" (inclination "locking," predicted by the Goldreich (1965) model for small inclinations and for uniform equinoctial precession) works also for nonuniform Colombo precession of the equator. Similarly, the variations of the equinoctial precession exert virtually no influence upon the satellite node dynamics: it regresses at an almost constant rate of  $\dot{\Omega}_{\text{near equatorial}} \approx 6.435 \text{ deg/yr}$ . The periape precession rate remains virtually constant, as shown in Fig. 3. The semimajor axis and eccentricity vary only slightly. Both in the near-equatorial case (as in Fig. 3) and the near-polar case (as in Fig. 5), this behaviour of  $a$  and  $e$  confirms the analytical predictions given by formula (44) in Efroimsky (2006), predictions that were derived from the appropriate planetary equations.

Consider a hypothetical Martian satellite initially set on a near-polar orbit:  $i_0 = 89 \text{ deg}$ . Similarly to the near-equatorial case, the variations of the equinoctial precession make virtually no influence upon the node regression, as seen in Figure 4. The "Goldreich lock," too, stays intact: the inclination is bounded within the interval  $88.65 \text{ deg} \leq i \leq 89.12 \text{ deg}$ . This is a kind of bonus: even though the Goldreich (1965) calculations are not designed to work at high inclinations (see the subsection below), the main outcome, the inclination "locking," remains valid even for near-polar orbits. On the other hand, in the behaviour of  $i$  we can see an unusual pattern – the "crankshaft" features (Fig. 9). The plots in Fig. 5 depict the time evolution of  $a$ ,  $e$ , and  $\omega$ . The node steadily regresses at a rate of  $\dot{\Omega}_{\text{near polar}} \approx 0.1227 \text{ deg/yr}$ . The manifest difference between  $\dot{\Omega}_{\text{near equatorial}}$  and  $\dot{\Omega}_{\text{near polar}}$  is very easily understood simply from looking at equation (5). We see that, very roughly,

$$\dot{\Omega} \approx -\frac{3}{2} n J_2 \left(\frac{\rho_e}{a}\right)^2 \frac{\cos i}{(1-e^2)^2} - \frac{\mu_n}{\sin i} \approx -\frac{3}{2} n J_2 \left(\frac{\rho_e}{a}\right)^2 \frac{\cos i}{(1-e^2)^2} - \dot{h}_p \cos I_p . \quad (37)$$

Plugging of the numbers indeed gives the values of  $\dot{\Omega}$  very close to those observed on Figure 2, for low  $i$ , and on Figure 4, for high  $i$ . Due to the smallness of  $\mu_n$ , the singular term with  $\sin i$  in the denominator causes problems only within the narrowest vicinity of the equator. (This singularity is not physical, but is merely a matter of our choice of the elements.) Similarly, for near-polar orbits, this terms plays a considerable role only in the closest vicinity (arc minutes) of

$i = \pi/2$ . This means that orbits so close to the pole may demonstrate behaviour different from what we saw in Figure 4. This phenomenon will be studied below.

To examine the precision of our semianalytical model implemented by equations (1 - 5) and (12 - 14), we have compared the above results with those stemming from a purely numerical integration performed in terms of Cartesian coordinates and velocities (see subsection 3.1). The necessity for this check was dictated, mainly, by the fact that within the semianalytical model the short-period terms are averaged out,<sup>4</sup> while the straightforward numerical integration of (32 - 33) neglects nothing. We carried out the comparison of the two methods over 20 Myr only. The outcomes, both for  $i_0 = 0.5$  degrees and  $i_0 = 89$  deg, were in a good agreement with the afore discussed results furnished by our semianalytical method. As an example, Fig. 6 shows the differences in inclination evolution in the case of  $i_0 = 0.5$  deg (top figure) and  $i_0 = 89$  deg (bottom figure) calculated by the semianalytical and by the purely numerical methods over 20 Myr. The differences in inclinations are normalized by the initial inclination, and the results are depicted in percent. It is seen that there is a good match between the models; in the  $i_0 = 0.5$  deg case the models match to within 1.3% while in the  $i_0 = 89$  deg the models match to within 0.3%.

All in all, the outcome of our computations is two-fold. First, we have made sure that the semianalytical model perfectly describes the dynamics over time scales of, at least, dozens of millions of years. Stated differently, the short-period terms and the terms of order  $O(\vec{\mu}^2)$  play no role over these time spans. Second, we have made sure that the “Goldreich lock” initially derived for very low inclinations and for uniform equinoctial precession, works well also for variable precession and even for high inclinations, at least in the above example with  $i_0 = 89$  deg.

### 3.2.3 Looking for trouble

A natural question arises as to whether the considered examples are representative. One may enquire if, perhaps, there still exists a combination of the initial conditions yielding noticeable variations of the satellite orbit inclination in the course of the primary’s variable equinoctial precession over vast spans of time. To answer this question, we should scan through all the possible combinations of initial conditions, to identify a particular combination that would entail a maximal inclination excursion relative to the initial inclination. Stated more formally, we should seek a set of initial conditions  $\{h_{p0}^*, I_{p0}^*, i_0^*, \Omega_0^*, \omega_0^*\}$  maximising the objective function  $|i(t) - i_0|$ :

$$\{h_{p0}^*, I_{p0}^*, i_0^*, \Omega_0^*, \omega_0^*\} = \arg \max_{\substack{t, h_{p0}, I_{p0} \\ i_0, \Omega_0, \omega_0}} |i(t) - i_0| \quad (38)$$

This problem belongs to the realm of optimisation theory. The optimisation space is constituted by the entire multitude of the permissible initial conditions. The sought after combination of initial conditions will be called *the optimal set*.

In this situation, the traditional optimisation schemes (such as the gradient search or the simplex method) may fail due to the rich dynamical structure of our problem: these methods may lead us to a local extremum. Thus, the search needs to be global. It can be carried out by means of Genetic Algorithms (GA’s) [14, 16, 17, 18]. These are wont to supersede the traditional optimisation procedures in the following aspects. First, instead of directly dealing with the parameters, the GA’s employ codings (usually, binary) of the parameter set (“strings,” in the GA terminology). Second, instead of addressing a single point of the optimisation space, the GA’s

---

<sup>4</sup> Be mindful that in equations (1 - 5) the exact  $\vec{\mu}$ -dependent terms are substituted with their orbital averages (12 - 14).

search from a population of the initial conditions. Third, instead of processing derivatives or whatever other auxiliary information, the GA's use only objective-function evaluations (“fitness evaluations”). Fourth, instead of deterministic rules to reiterate, the GA's rely upon probabilistic transition rules. Additional details on the particular GA mechanism used herein can be found in Appendix B.

A GA optimisation was implemented using the parameter values given in Table 5. The search

parameters	numerical values
Population size	30
Number of generations	100
String length	16 bit
Probability of crossover	0.99
Probability of mutation	0.02

Table 5: Parameter values used for the GA optimization

for the inclination-maximising initial conditions resulted in the following set:

$$I_{p0}^* = 5.0936 \text{ deg}, \quad h_{p0}^* = 54.9 \text{ deg}, \quad i_0^* = 90.7049 \text{ deg}, \quad \Omega_0^* = 223.1556 \text{ deg}, \quad \omega_0^* = 91.2836 \text{ deg} \quad . \quad (39)$$

Thus, the initial orbit is *retrograde* and, not surprisingly, *very-near-polar*. (See the discussion after formula (37).) The resulting time histories for a 1 Byr integration are depicted in Fig. 7, for  $i$  and  $\Omega$ . In both cases the inclination amplitude is relatively large,  $\max_t |i(t) - i_0| \approx 1 \text{ deg}$ , but qualitatively, it still complies with inclination locking.

Here again, a comparison of the semianalytical theory with the pure numerical integration was carried out, and it completely confirmed this weak chaotic behaviour.

## 4 Comparison of the numerical calculations and Goldreich's model

The final step in our study will be to compare the semianalytical model to Goldreich's approximation (22 - 26). To that end, we simulate our semianalytical model, using the initial conditions (39), for a 20 Myr time scale and compare the outcome with that resulting from Goldreich's approximation simulated with the same initial conditions. The results of this comparison are depicted in Figs. 8 - 9. Specifically, Fig. 8 compares the time histories of  $I_p$  and  $h_p$ . The evolution of the equator's node  $h_p$  is virtually the same in both models, but there are noticeable differences in the dynamics of  $I_p$ . While Goldreich's approximation assumes a constant  $I_p$ , the semianalytical model is based on the Colombo calculation of the equinoctial precession, calculation that predicts considerable oscillations within the range  $2.99 \text{ deg} \leq I_p \leq 13.61 \text{ deg}$ . This entails the difference between the dynamics predicted by our semianalytical model and the dynamics stemming from the Goldreich approximation. These differences, for  $i$  and  $\Omega$ , are depicted in Fig. 9. In Goldreich's model,  $i$  stays extremely close to the initial value,  $90.39 \text{ deg} \leq i \leq 90.74 \text{ deg}$ , which is the essence of the *Goldreich lock*. However, in the more accurate, semianalytical model we have  $88.94 \text{ deg} \leq i \leq 91 \text{ deg}$ . The time history of  $\Omega$ , too, reveals that Goldreich's approximation does not adequately model the actual dynamics, since it predicts a much larger secular change than the semi-analytical model.

All in all, the dynamics (i.e., particular trajectories) predicted by the two models are quantitatively different. At the same time, when it comes to the most physically important conclusion from the Goldreich approximation, the “Goldreich lock,” one may still say that, qualitatively, the semianalytical model confirms its existence even for variable equinoctial precession, and even for highly inclined satellite orbits. It is, though, not as stiff as predicted by the Goldreich model: we can see from Fig. 9 that the orbit inclination varies within a two-degree span, while the Goldreich approximation would constrain it to small shares of a degree.

An intriguing fine feature of the inclination evolution, which manifests itself for orbits close to polar, is the “crankshaft” feature. This kind of behaviour, well defined in Fig. 9, is not rendered by the Goldreich model, because that model was initially developed for small inclinations. One might suspect that the “crankshaft” is merely a numerical artefact, had it not been discovered under different circumstances (in the absence of precession but in the presence of a third body) by Zhang & Hamilton (2005). This kind of pattern may be generic for the close vicinity of  $i = 90$  deg. In our case, the approximate formula (37) drops us a hint that the dynamics may become unexpected on a very close approach to  $i = 90$  deg, when the second term becomes dominant in the right-hand side of (37). Whether the “crankshaft” feature is a physical effect in its own right, should be examined by means of a more comprehensive model that includes the tides. This work will be done in Efroimsky, Gurfil & Lainey (2007).

## 5 Conclusions

In the article thus far, we continued developing a tool for exploring long-term evolution of a satellite orbit about a precessing oblate primary. In particular, we were interested in the time-dependence of the orbit inclination relative to the moving equator of date. The problem was approached using different methods. One, semianalytical, was based on numerical integration of simplified and averaged Lagrange-type equations for the secular parts of the Keplerian orbital elements introduced in a noninertial reference frame coprecessing with the planetary equator of date. These five equations, (1 - 5), were borrowed from Efroimsky (2006). The other approach was a straightforward, purely numerical, computation of the satellite dynamics using Cartesian coordinates in the J1950 inertial reference frame.

The results of both computations have demonstrated a perfect agreement over 20 Myr. This means that the semianalytical model perfectly describes the dynamics over time spans of, at least, dozens of millions of years. This means, among other things, that the terms neglected in the semianalytical model (the short-period terms and the terms of order  $O(\vec{\mu}^2)$ ) play no significant role on these time scales.

Our calculations have shown the advantages and the limitations of the simple model developed by Goldreich (1965) for uniform equinoctial precession and low inclinations. Though his model does not adequately describe the dynamics (that turns out to be weakly chaotic), the main physical prediction of Goldreich’s model – the “Goldreich lock” – sustains the variations of equinoctial precession. To some extent, this prediction remains valid even at large inclinations: variations of the satellite orbit inclination on the precessing equator of date always remain small – dozens of arcseconds, for low-inclination orbits, and about two angular degrees, for high-inclination orbits.

A subtle feature in the inclination dynamics, feature that is not accounted for by the Goldreich model, is the “crankshaft” that shows itself for near-polar orbits (Fig. 7 and Fig. 9). To safely claim that this feature is physical, we shall have to check it with the tidal forces brought into consideration. (Efroimsky, Gurfil & Lainey 2007)

## Appendix A: Closed-Form Expressions for $\dot{\mu}_1, \dot{\mu}_2, \dot{\mu}_3$

Using the compact notation  $c_{(\cdot)} \equiv \cos(\cdot)$  and  $s_{(\cdot)} \equiv \sin(\cdot)$ , and conforming to the procedure described in the text, we obtain the following expressions for  $\dot{\mu}_1, \dot{\mu}_2, \dot{\mu}_3$ :

$$\begin{aligned}
\dot{\mu}_1 = & (((6p^2q^2 - p^4 - q^4)(c_{I_p})^3 + (-6p^2q^2 + p^4 + q^4)c_{I_p})(c_{h_p})^4 \\
& + ((-3p^4 - 6p^2q^2 - 3q^2 + 3p^2 + 5q^4)(c_{I_p})^3 + (2p^4 - 4q^4 + 6p^2q^2 - 2p^2 + 2q^2)c_{I_p}) \\
& \cdot (c(h_p))^2 + (3q^2 - 3p^2q^2 - 4q^4)(c_{I_p})^3 + (3q^4 - 2q^2 + 2p^2q^2)c_{I_p} \\
& + (((4qp^3 - 4q^3p)(c_{I_p})^3 + (4q^3p - 4qp^3)c_{I_p})(c_{h_p})^5 + ((2qp^3 - 6qp + 14q^3p)(c_{I_p})^3 \\
& + (-12q^3p + 4qp)c_{I_p})(c_{h_p})^3 + ((6qp - 10q^3p - 6qp^3)(c_{I_p})^3 + (4qp^3 + 8q^3p - 4qp)c_{I_p})c_{h_p}) \\
& \cdot (s_{h_p})^{-1}(s_{I_p})^{-1} + (((-9pq^2 + 9pq^4 - 3p^5 + 3p^3 + 6p^3q^2)(c_{I_p})^2 + 3pq^2 - 2p^3q^2 + p^5 \\
& - 3pq^4 - p^3)(c_{h_p}^3 + ((-11p^3q^2 - p^5 - 10pq^4 - p + 2p^3 + 11pq^2)(c(I_p))^2 + 3pq^4 + 3p^3q^2 \\
& - 3pq^2)c_{h_p} + (((-9p^2q + 6p^2q^3 + 9p^4q - 3q^5 + 3q^3)(c_{I_p})^2 - 3p^4q + 3p^2q - 2p^2q^3 \\
& - q^3 + q^5)(c_{h_p}^4 + ((7p^2q - p^2q^3 - 8q^3 - 8p^4q + 7q^5 + q)(c_{I_p})^2 - 2q^5 + p^2q^3 + 2q^3 \\
& + 3p^4q - 3p^2q)(c(h_p))^2 + (5q^3 - 4q^5 - q - 5p^2q^3 - p^4q + 2p^2q)(c_{I_p})^2 - q^3 + q^5 + p^2q^3) \\
& \cdot (s(h_p))^{-1}) \left[ \sqrt{1 - p^2 - q^2} \right]^{-1})\alpha^2 - \alpha((( -2q\dot{p} - 2\dot{q}p)(c_{I_p})^2 + 2q\dot{p} + 2\dot{q}p)(c_{h_p})^2 \\
& + (\dot{q}p + q\dot{p})(c_{I_p})^2 - \dot{q}p - qp\dot{p} + ((( -2p\dot{p} + 2q\dot{q})(c_{I_p})^2 + 2p\dot{p} - 2q\dot{q})(c_{h_p})^3 + ((2p\dot{p} - 2q\dot{q})(c_{I_p})^2 \\
& - 2p\dot{p} + 2q\dot{q})c_{h_p})(s(h_p))^{-1}(s(I_p))^{-1} + (( -\dot{q}p^2 - 2q^2\dot{q} + \dot{q} - qp\dot{p})c_{I_p}c_{h_p} \\
& + \frac{(\dot{p} - 2p^2\dot{p} - pq\dot{q} - \dot{p}q^2)c_{I_p}(c_{h_p})^2 + (-\dot{p} + \dot{p}q^2 + 2p^2\dot{p} + pq\dot{q})c_{I_p}}{s_{h_p}}) \left[ \sqrt{1 - p^2 - q^2} \right]^{-1}) \quad , \quad (40)
\end{aligned}$$

$$\begin{aligned}
\dot{\mu}_2 = & (((4q^3p - 4qp^3)(c_{I_p})^2 + 4qp^3 - 4q^3p)(c_{h_p})^4 \\
& + ((qp^3 - 7q^3p + 2qp)(c_{I_p})^2 - 3qp^3 + 5q^3p)(c_{h_p})^2 + (2q^3p - qp + qp^3)(c_{I_p})^2 \\
& - q^3p + (((6p^2q^2 - p^4 - q^4)(c_{I_p})^2 - 6p^2q^2 + p^4 + q^4)(c_{h_p}^5 + ((3q^4 - q^2 - 9p^2q^2 + p^2)(c_{I_p})^2 \\
& - p^4 - 2q^4 + 9p^2q^2)(c_{h_p})^3 + (( -p^2 + q^2 - 2q^4 + p^4 + 3p^2q^2)(c(I_p))^2 + q^4 \\
& - 3p^2q^2)c(h_p))(s_{h_p})^{-1}(s(I_p))^{-1} + (( -4p^2q^3 + 6p^2q - 2q^3 + 2q^5 - 6p^4q)c(I_p)(c_{h_p})^3 \\
& + (2q^3 + 4p^4q + 2p^2q^3 - 4p^2q - 2q^5)c_{I_p}c_{h_p} + (( -2p^5 - 6pq^2 + 6pq^4 + 4p^3q^2 + 2p^3)c_{I_p}(c_{h_p})^4 \\
& + (2p^5 + 8pq^2 - 8pq^4 - 6p^3q^2 - 2p^3)c_{I_p}(c_{h_p})^2 + (2pq^4 - 2pq^2 + 2p^3q^2)c_{I_p})(s_{h_p})^{-1}) \\
& \cdot \left[ \sqrt{1 - p^2 - q^2} \right]^{-1})\alpha^2 - \alpha(((2p\dot{p} - 2q\dot{q})(c_{I_p})^3 + (-2p\dot{p} + 2q\dot{q})c_{I_p})(c_{h_p}^2 \\
& + (2p\dot{p} + 4q\dot{q})(c_{I_p})^3 + (-2p\dot{p} - 4q\dot{q})c_{I_p} + ((( -2q\dot{p} - 2\dot{q}p)(c_{I_p})^3 + (2q\dot{p} + 2\dot{q}p)c_{I_p})(c_{h_p})^3 \\
& + ((2q\dot{p} + 2\dot{q}p)(c(I_p))^3 + (-2q\dot{p} - 2\dot{q}p)c_{I_p})c(h_p))(s_{h_p})^{-1}(s(I_p))^{-1} \\
& + (((2\dot{p}q^2 + 2pq\dot{q} + 4p^2\dot{p} - 2\dot{p})(c_{I_p})^2 + \dot{p} - 2p^2\dot{p} - pq\dot{q} - \dot{p}q^2)c_{h_p} \\
& + ((( -2q\dot{p} - 2\dot{q}p^2 - 4q^2\dot{q} + 2\dot{q})(c_{I_p})^2 - \dot{q} + \dot{q}p^2 + 2q^2\dot{q} + qp\dot{p})(c_{h_p}^2 \\
& + (2q\dot{p} - 2\dot{q} + 2\dot{q}p^2 + 4q^2\dot{q})(c_{I_p})^2 - \dot{q}p^2 - 2q^2\dot{q} + \dot{q} - qp\dot{p})(s(h_p))^{-1}) \left[ \sqrt{1 - p^2 - q^2} \right]^{-1}) \quad , \quad (41)
\end{aligned}$$

and

$$\begin{aligned}
\dot{\mu}_3 = & (((4q^3p - 4qp^3)(c_{I_p})^2 + 4qp^3 - 4q^3p)(c_{h_p})^4 + ((qp^3 - 7q^3p + 2qp)(c(I_p))^2 \\
& - 3qp^3 + 5q^3p)(c_{h_p})^2 + (2q^3p - qp + qp^3)(c_{I_p})^2 - q^3p + (((6p^2q^2 - p^4 - q^4)(c_{I_p})^2 - 6p^2q^2 + p^4 \\
& + q^4)(c(h_p))^5 + ((3q^4 - q^2 - 9p^2q^2 + p^2)(c_{I_p})^2 - p^4 - 2q^4 + 9p^2q^2)(c_{h_p})^3 + ((-p^2 + q^2 - 2q^4 \\
& + p^4 + 3p^2q^2)(c(I_p))^2 + q^4 - 3p^2q^2)c(h_p)(s_{h_p})^{-1})(s(I_p))^{-1} + ((-4p^2q^3 + 6p^2q - 2q^3 + 2q^5 \\
& - 6p^4q)c(I_p)(c_{h_p})^3 + (2q^3 + 4p^4q + 2p^2q^3 - 4p^2q - 2q^5)c_{I_p}c_{h_p} \\
& + ((-2p^5 - 6pq^2 + 6pq^4 + 4p^3q^2 + 2p^3)c_{I_p}(c_{h_p})^4 + (2p^5 + 8pq^2 - 8pq^4 - 6p^3q^2 - 2p^3)c_{I_p}(c_{h_p})^2 \\
& + (2pq^4 - 2pq^2 + 2p^3q^2)c_{I_p})(s_{h_p})^{-1})\sqrt{1 - p^2 - q^2}^{-1})\alpha^2 - \alpha(((2p\dot{p} - 2q\dot{q})(c_{I_p})^3 \\
& + (-2p\dot{p} + 2q\dot{q})(c(I_p))^2 + (2p\dot{p} + 4q\dot{q})(c_{I_p})^3 + (-2p\dot{p} - 4q\dot{q})c_{I_p} \\
& + (((-2q\dot{p} - 2\dot{q}p)(c_{I_p})^3 + (2q\dot{p} + 2\dot{q}p)c_{I_p})(c_{h_p})^3 + ((2q\dot{p} + 2\dot{q}p)(c(I_p))^3 \\
& + (-2q\dot{p} - 2\dot{q}p)c_{I_p})(c(h_p))^{-1})(s_{I_p})^{-1} + (((2\dot{p}q^2 + 2pq\dot{q} + 4p^2\dot{p} - 2\dot{p})(c_{I_p})^2 + \dot{p} \\
& - 2p^2\dot{p} - pq\dot{q} - \dot{p}q^2)c_{h_p} + (((-2qpp - 2\dot{q}p^2 - 4q^2\dot{q} + 2\dot{q})(c(I_p))^2 - \dot{q} + \dot{q}p^2 + 2q^2\dot{q} \\
& + qpp)(c_{h_p})^2 + (2qpp - 2\dot{q} + 2\dot{q}p^2 + 4q^2\dot{q})(c_{I_p})^2 - \dot{q}p^2 - 2q^2\dot{q} + \dot{q} - qpp)(s_{h_p})^{-1}) \\
& \cdot \left[ \sqrt{1 - p^2 - q^2} \right]^{-1}) \quad (42)
\end{aligned}$$

## Appendix B: Niching Genetic Algorithms

The most commonly used Genetic Algorithm (GA) is the so-called “Simple GA.” To perform an evolutionary search, the Simple GA uses the operators of crossover, reproduction, and mutation. A crossover is used to create new solution strings (“children” or “offspring”) from the existing strings (“parents”). Reproduction copies individual strings according to the objective function values. Mutation is an occasional random alteration of the value of a string position, used to promote diversity of solutions.

Although Simple GA’s are capable of detecting the global optimum, they suffer from two main drawbacks. First, convergence to a local optimum is possible due to the effect of premature convergence, where all individuals in a population become nearly identical before the optima has been located. Second, convergence to a single optimum does not reveal other optima, which may exhibit attractive features. To overcome these problems, modifications of Simple GA’s were considered. These modifications are called niching methods, and are aimed at promoting a diversity of solutions for multi-modal optimisation problems. In other words, instead of converging to a single (possibly local) optimum, niching allows for a number of optimal solutions to co-exist, and it lets the designer choose the appropriate one. The niching method used throughout this study is that of Deterministic Crowding. According to this method, individuals are first randomly grouped into parent pairs. Each pair generates two children by application of the standard genetic operators. Every child then competes against one of his parents. The winner of the competition moves on to the next generation. By using the notation  $P_i$  for a parent,  $C_i$  for a child,  $f(\cdot)$  for a fitness, and  $d(\cdot)$  for a distance, a pseudo-code for the two possible parent-child tournaments can be written as follows:

If  $[d(P_1, C_1) + d(P_2, C_2) = d(P_1, C_2) + d(P_2, C_1)]$   
If  $f(C_1) \geq f(P_1)$  replace  $P_1$  with  $C_1$   
If  $f(C_2) \geq f(P_2)$  replace  $P_2$  with  $C_2$

Else

If  $f(C_1) \geq f(P_2)$  replace  $P_2$  with  $C_1$   
If  $f(C_2) \geq f(P_1)$  replace  $P_1$  with  $C_2$

In addition to applying the Deterministic Crowding niching method, we used a two-point crossover instead of a single-point one. In the Simple GA, the crossover operator breaks the binary string of parameters, the “chromosome,” at a random point and exchanges the two pieces to create a new “chromosome.” In a two-point crossover, the “chromosome” is represented with a ring. The string between the two-crossover points is then exchanged. The two-point crossover or other multiple-point crossover schemes have preferable properties when optimisation highly nonlinear functions is performed.

## Acknowledgments

ME is grateful to George Kaplan for numerous fruitful discussions on the subject, and to Marc Murison for a consultation on the possible scenario of the Martian satellites capture. The work of ME was supported by NASA grant W-19948. The work of VL was supported by the European Community’s Improving Human Potential Programme contract RTN2-2001-00414 MAGE.

## References

- [1] Brouwer, D. 1959. “Solution of the problem of artificial satellite theory without drag.” *The Astronomical Journal*, Vol. **64**, pp. 378 - 397.
- [2] Brumberg, V. A., Evdokimova, L. S.; & Kochina N. G. 1971. “Analytical Methods for the Orbits of Artificial Satellites of the Moon.” *Celestial Mechanics*, Vol. **3**, pp. 197 - 221.
- [3] Colombo, G. 1966. “Cassini’s second and third laws.” *The Astronomical Journal.*, Vol. **71** pp. 891 - 896.
- [4] Efroimsky, Michael. 2002a. “Equations for the orbital elements. Hidden symmetry.” Preprint No 1844 of the Institute of Mathematics and its Applications, University of Minnesota <http://www.ima.umn.edu/preprints/feb02/feb02.html>
- [5] Efroimsky, Michael. 2002b. “The Implicit Gauge Symmetry Emerging in the N-body Problem of Celestial Mechanics.” [astro-ph/0212245](http://arxiv.org/abs/astro-ph/0212245)
- [6] Efroimsky, M.; & Goldreich, P. 2003. “Gauge Symmetry of the N-body Problem in the Hamilton-Jacobi Approach.” *Journal of Mathematical Physics*, Vol. **44**, pp. 5958 - 5977 [astro-ph/0305344](http://arxiv.org/abs/astro-ph/0305344)
- [7] Efroimsky, M., & P. Goldreich. 2004. “Gauge Freedom in the N-body Problem of Celestial Mechanics.” *Astronomy & Astrophysics*, Vol. **415**, pp. 1187 - 1199 [astro-ph/0307130](http://arxiv.org/abs/astro-ph/0307130)
- [8] Efroimsky, M. 2004a. “On the theory of canonical perturbations and its application to Earth rotation. A source of inaccuracy in the calculation of angular velocity.” Talk at the conference

“Journées 2004: Systèmes de référence spatio-temporels,” l’Observatoire de Paris, 20 - 22 September 2004. astro-ph/0409282

[9] Efroimsky, M. 2004b. “Long-term evolution of orbits about a precessing oblate planet. 1. The case of uniform precession.”

astro-ph/0408168

This preprint is a very extended version of Efroimsky (2005). It contains a lengthy Appendix where all the necessary analytical calculations are explained in every detail.

[10] Efroimsky, M. 2005. “Long-term evolution of orbits about a precessing oblate planet: 1. The case of uniform precession.” *Celestial Mechanics and Dynamical Astronomy*, Vol. **91**, pp. 75 - 108.

[11] Efroimsky, M. 2006. “Long-term evolution of orbits about a precessing oblate planet: 2. The case of variable precession.” To be published in *Celestial Mechanics & Dynamical Astronomy*. astro-ph/0607522

[12] Efroimsky, M., Gurfil, P., & Lainey, V. 2007. “Long-term evolution of orbits about a precessing oblate planet: 4. A comprehensive model.” In preparation.

[13] Everhart, E. 1985. “An efficient integrator that uses Gauss-Radau spacings.” *Dynamics of Comets: Their Origin and Evolution. Proceedings of IAU Colloquium 83 held in Rome on 11 - 15 June 1984*. Edited by A. Carusi and G. B. Valsecchi. Dordrecht: Reidel, Astrophysics and Space Science Library. Vol. **115**, p. 185 (1985)

[14] Goldberg, D. E., *Genetic Algorithms in Search, Optimization and Machine Learning*, Addison-Wesley, Reading, MA, 1989.

[15] Goldreich, P. 1965. ”Inclination of satellite orbits about an oblate precessing planet.” *The Astronomical Journal*, Vol. **70**, p. 5 - 9

[16] Gurfil, P., Kasdin, N. J., Arrell, R. J., Seager S., & Nissanke, S. 2002. “Infrared Space Observatories: How to Mitigate Zodiacal Dust Interference.” *The Astrophysical Journal*, Vol. **567**, pp. 1250 - 1261.

[17] Gurfil, P., & Kasdin, N. J. 2002. “Characterization and Design of Out-of-Ecliptic Trajectories Using Deterministic Crowding Genetic Algorithms.” *Computer Methods in Applied Mechanics and Engineering*, Vol. **191**, pp. 2169 - 2186.

[18] Gurfil, P., & Kasdin, N. J. 2002. “Niching Genetic Algorithms-Based Characterization of Geocentric Orbits in the 3D Elliptic Restricted Three-Body Problem.” *Computer Methods in Applied Mechanics and Engineering*, Vol. **191**, pp. 5673 - 5696.

[19] Kinoshita, H. 1977. “Theory of the Rotation of the Rigid Earth.” *Celestial Mechanics*, Vol. **15**, pp. 277 - 326.

[20] Kozai, Y. 1960. “Effect of precession and nutation on the orbital elements of a close earth satellite.” *The Astronomical Journal*, Vol. **65**, pp. 621 - 623.

[21] Lainey, V., Duriez, L. & Vienne, A. 2004. “New accurate ephemerides for the Galilean satellites of Jupiter. I. Numerical integration of elaborated equations of motion.” *Astronomy & Astrophysics*, Vol. **420**, pp. 1171 - 1183.

[22] Lambeck, K., 1980. *The Earth's Variable Rotation: Geophysical Causes and Consequences*. Cambridge University Press, London 1980.

[23] Laskar, J. 1988. "Secular evolution of the solar system over 10 million years." *Astronomy & Astrophysics*, Vol. **198**, pp. 341 - 362.

[24] Laskar, J., & J. Robutel. 1993. "The Chaotic Obliquity of the Planets." *Nature*, Vol. **361**, pp. 608 - 612.

[25] Murison, M. 1988. "Satellite Capture and the Restricted Three-Body Problem." Ph.D. Thesis, University of Wisconsin, Madison 1988.

[26] Newman, W., & M. Efroimsky. 2003. "The Method of Variation of Constants and Multiple Time Scales in Orbital Mechanics." *Chaos*, Vol. 13, pp. 476 - 485.

[27] Pang, K. D., J. B. Pollack, J. Veverka, A. L. Lane, & J. M. Ajello. 1978. "The Composition of Phobos: Evidence for Carbonateous Chondrite Surface from Spectral Analysis." *Science*, Vol. **199**, p. 64

[28] Pollack, J. B.; Burns, J. A.; & Tauber, M. E. 1979. "Gas Drag in Primordial Circumplanetary Envelopes. A Mechanism for Satellite Capture." *Icarus*, Vol. **37**, p. 587

[29] Proskurin, V. F., & Batrakov, Y. V. 1960. "Perturbations of the Motion of Artificial Satellites, caused by the Earth Oblateness." *The Bulletin of the Institute of Theoretical Astronomy*, Vol. **7**, pp. 537 - 548.

[30] Smith, D. E.; Lemoine, F. G.; Zuber, M. T. 1995. "Simultaneous estimation of the masses of Mars, Phobos, and Deimos using spacecraft distant encounters," *Geophysical Research Letters*, Vol. **22**, pp. 2171 - 2174.

[31] Szebehely, V. 1967. *Theory of Orbits*. Academic Press, NY.

[32] Tolson, R. H., and 15 collaborators. 1978. "Viking First Encounter of Phobos. Preliminary Results." *Science*, Vol. **199**, p. 61

[33] Touma, J., & J. Wisdom. 1994. "Lie-Poisson Integrators for Rigid Body Dynamics in the Solar System." *The Astronomical Journal*, Vol. **107**, pp. 1189 - 1202.

[34] Veverka, J. 1977. "Phobos and Deimos." *Scientific American*, Vol. **236**, p. 30

[35] Ward, W. 1973. "Large-scale Variations in the Obliquity of Mars." *Science*. Vol. **181**, pp. 260 - 262.

[36] Ward, W. 1974. "Climatic Variations of Mars. Astronomical Theory of Insolation." *Journal of Geophys. Research*, Vol. **79**, pp. 3375 - 3386.

[37] Ward, W. 1979. "Present Obliquity Oscillations of Mars - Fourth-order Accuracy in Orbital e and i." *Journal of Geophys. Research*, Vol. **84**, pp. 237 - 241.

[38] Ward, W. 1982. "Comments on the long-term Stability of the Earth's Obliquity." *Icarus*, Vol. **50**, pp. 444 - 448.

[39] Zhang, K., & Hamilton, D. P. 2005. "Dynamics of Inner Neptunian Satellites." Abstracts of the 37th DPS Meeting of the American Astronomical Society. In: AAS Bulletin, Vol. **37**, pp. 667 - 668

## Figures

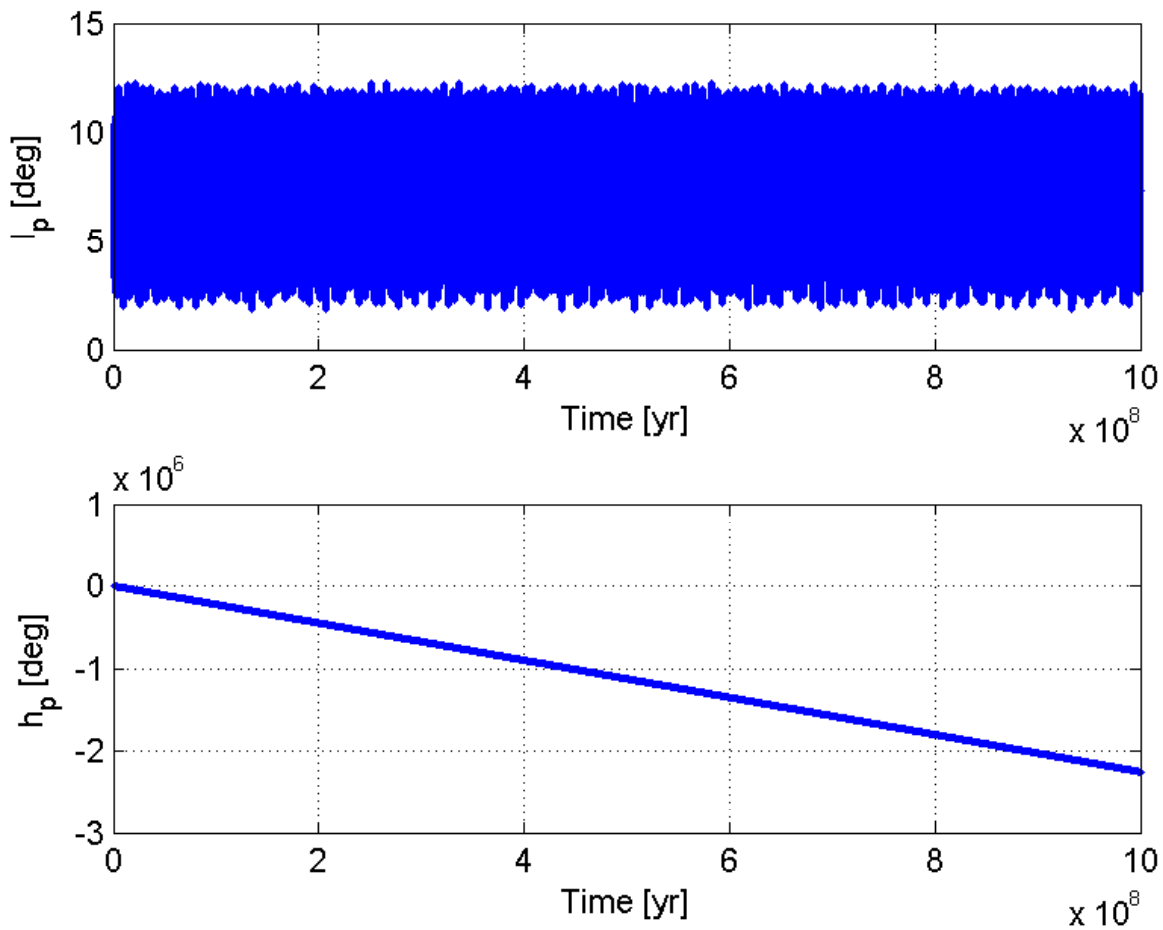


Figure 1: Evolution of the inclination and of the longitude of the node of the Martian equator of date relative to the equator of epoch, over 1 Byr, in the Colombo approximation.

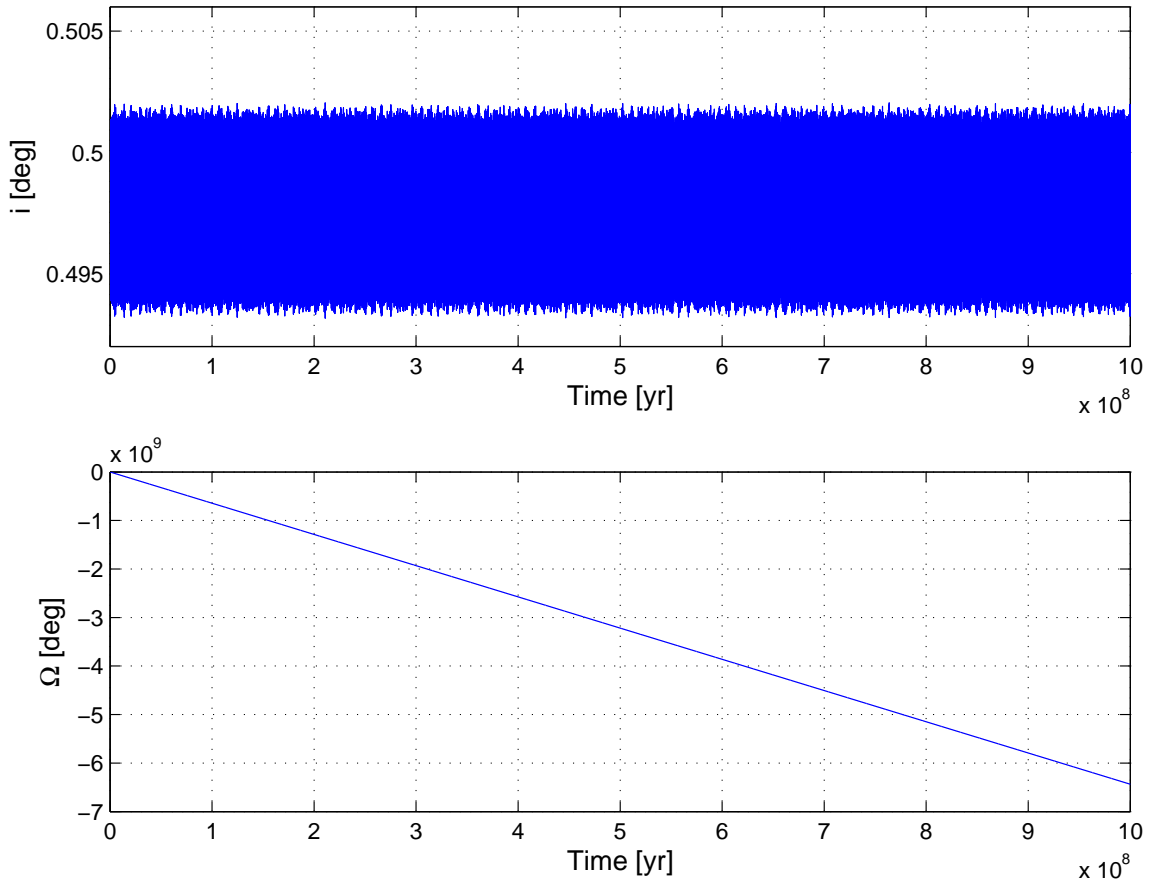


Figure 2: Evolution of the inclination (initially set to 0.5 degree) and of the longitude of the node of Deimos over 1 Byr. The plot, obtained by integration of the semianalytical model, exhibits inclination locking and uniform regression of the node.

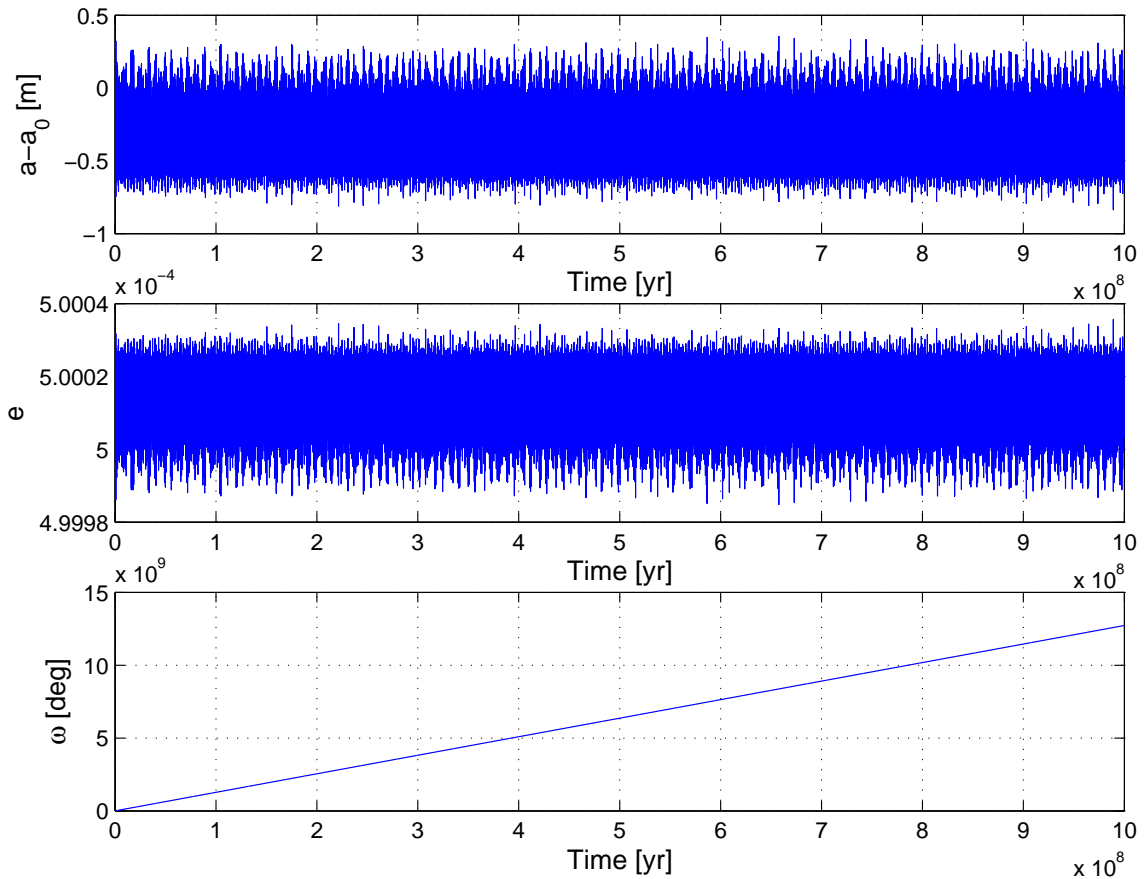


Figure 3: Evolution of the semimajor axis, eccentricity, and argument of periapsis of Deimos over 1 Byr. (The inclination was initially set to 0.5 degree.) Both the semimajor axis and eccentricity exhibit periodic motion about their initial values. (The variations of the semimajor axis are so small that it is more convenient to plot  $a - a_o$  rather than  $a$ .) The plots were obtained by integration of the semianalytical model.

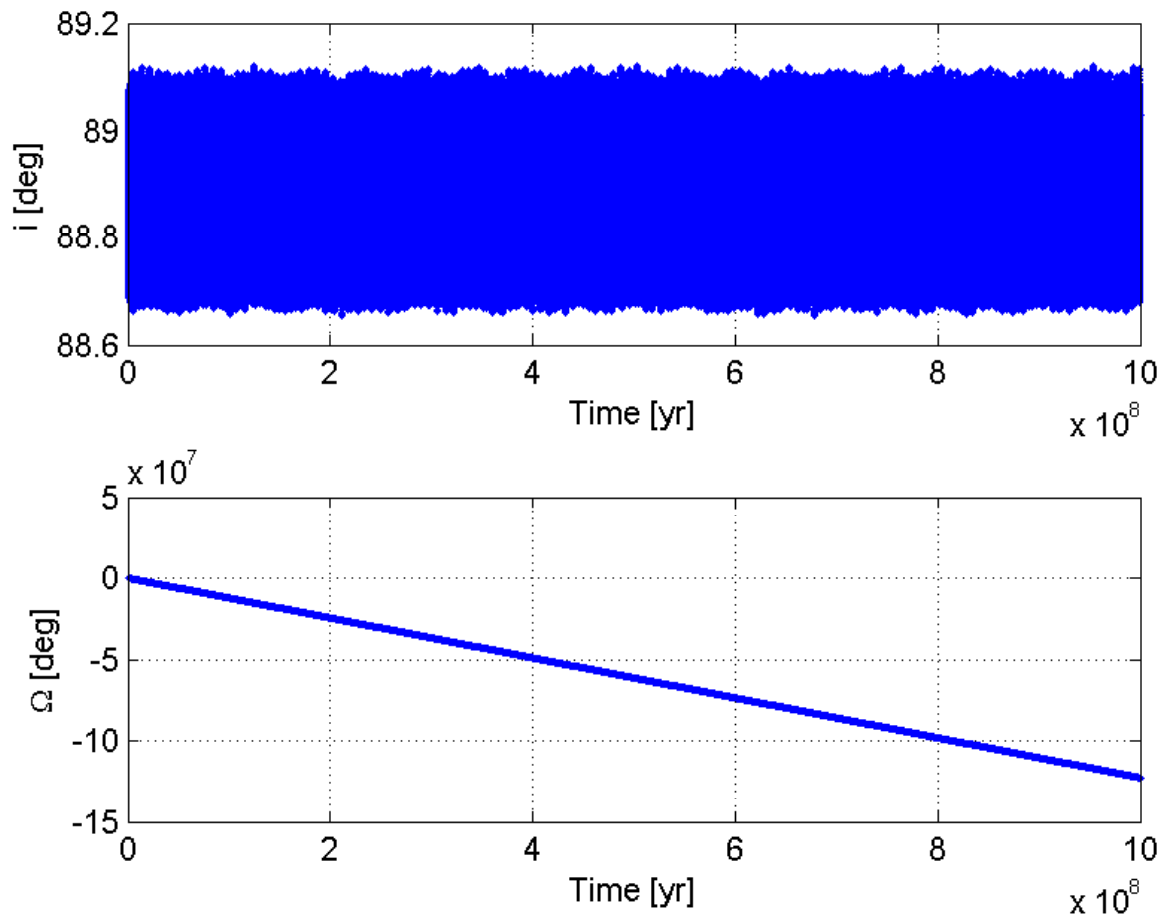


Figure 4: Evolution of the inclination and of the longitude of the node of Deimos over 1 Byr. (The inclination was initially set to 89 degrees.) The plot, obtained by integration of the semianalytical model, exhibits inclination locking and uniform regression of the node.

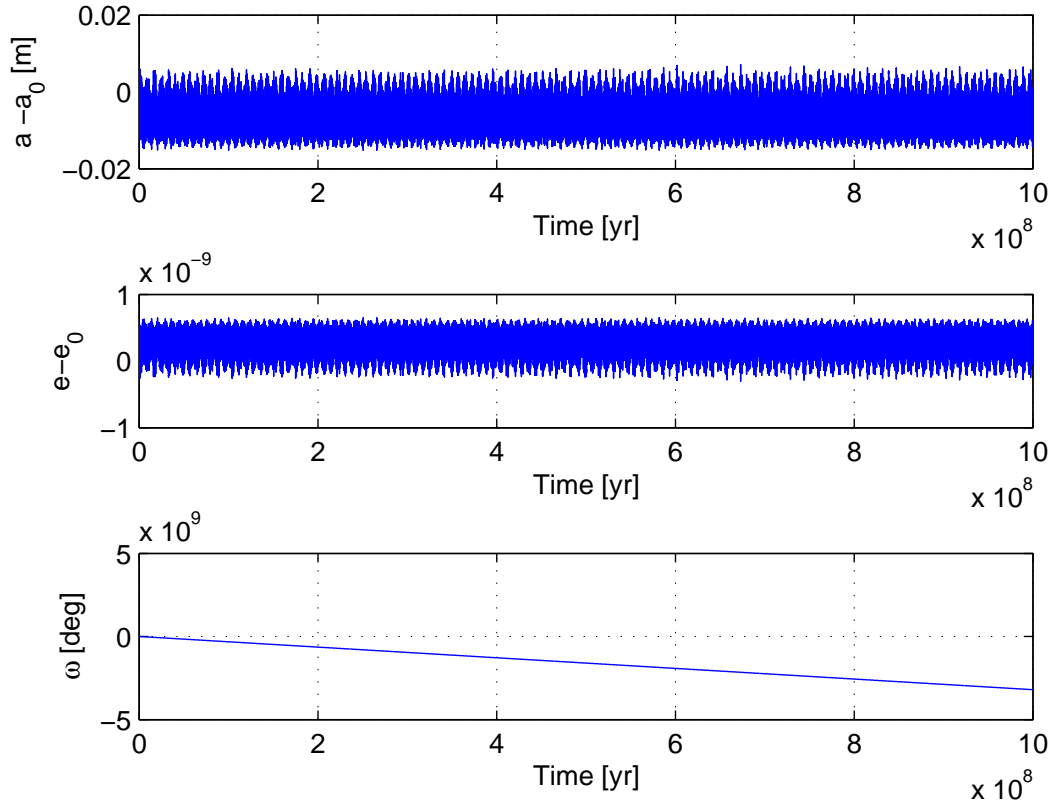


Figure 5: Evolution of the semi-major axis, eccentricity, and argument of periapsis of Deimos over 1 Byr. (The inclination was initially set to 89 degrees.) The semi-major axis and eccentricity exhibit long-periodic motion about the initial value. (The variations of the semimajor axis are so small that it is more convenient to plot  $a - a_0$  rather than  $a$ .) The plots were obtained by integration of the semianalytical model.

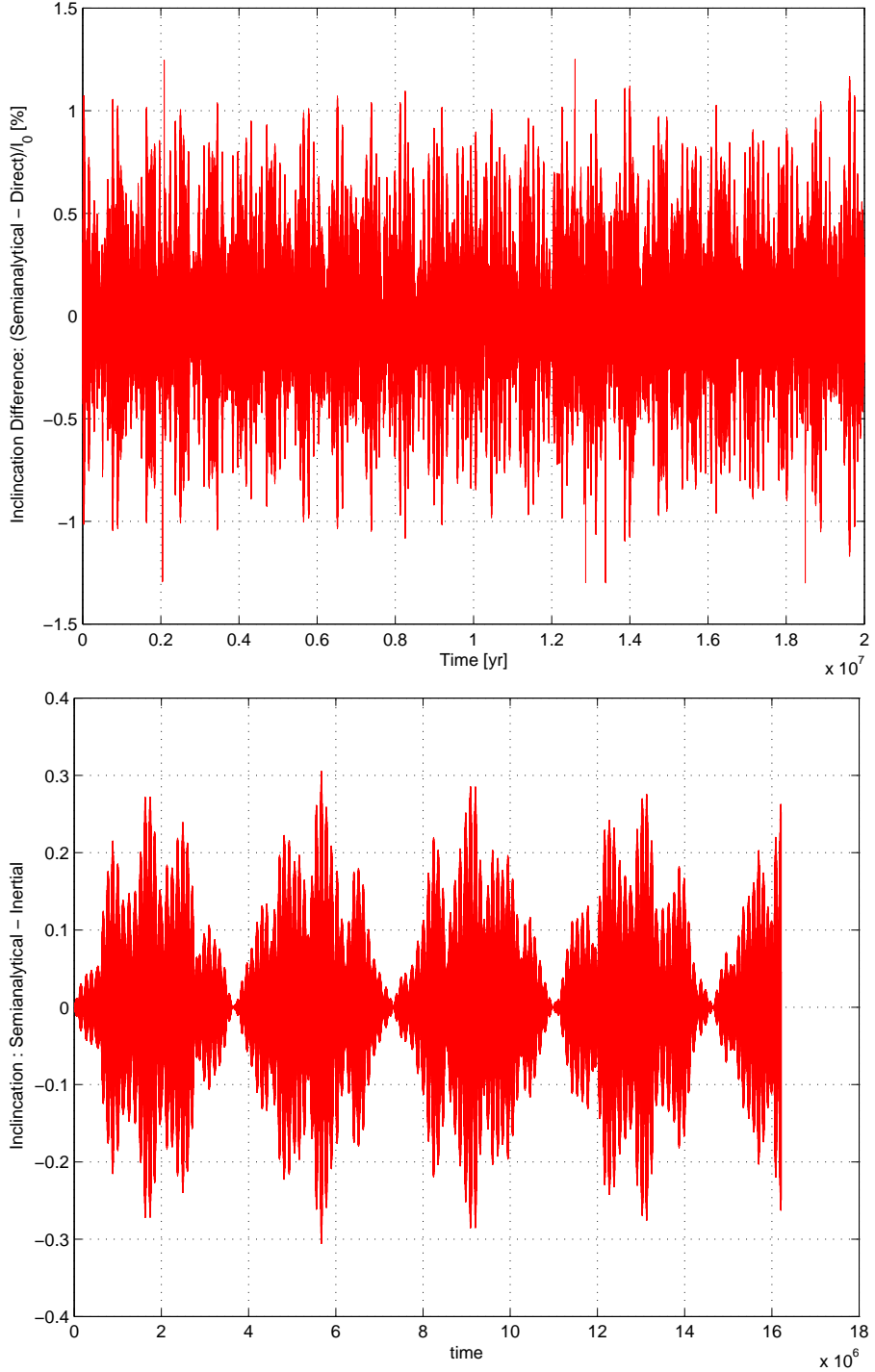


Figure 6: Comparison of the semi-analytical model to a purely numerical integration. The plot shows the differences in inclination as predicted by the two models, normalised by the initial inclination. The top plot shows the case of the initial inclination  $i_o = 0.5$  deg. In this case, the difference between the two models stays within less than 1.3% for over 20Myr. The bottom plot depicts the case of  $i_o = 89$  deg. In this case, the difference between the two models stays within less than 0.3% for over 20Myr.

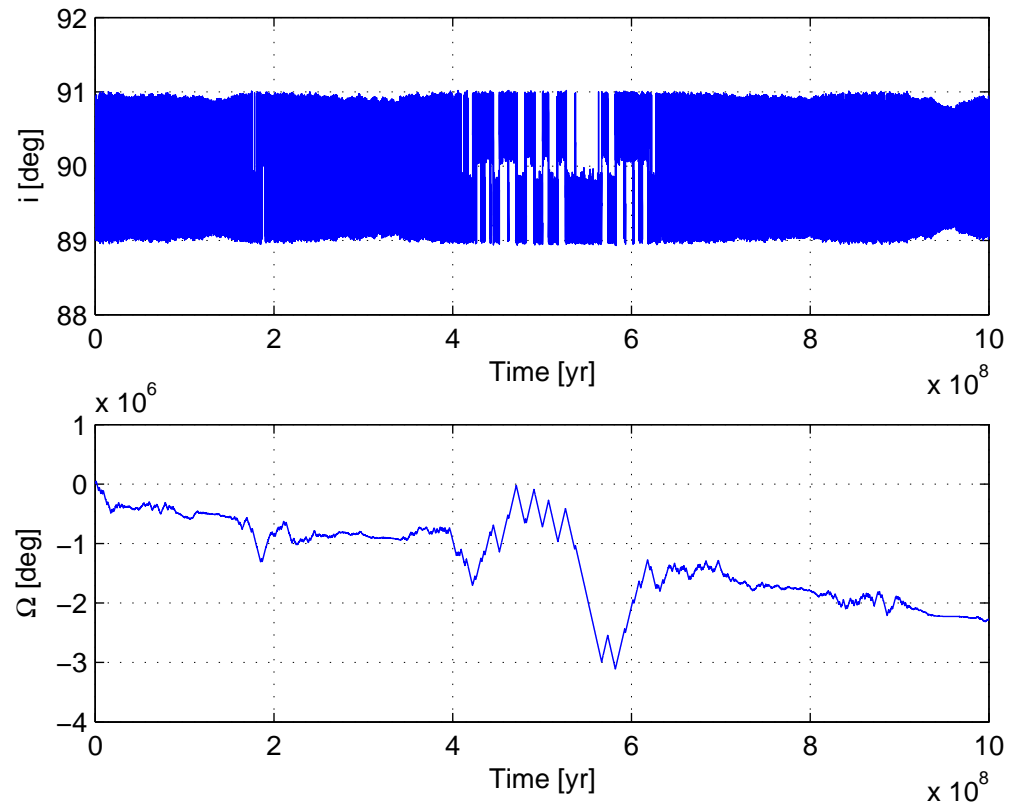


Figure 7: Evolution of the inclination and longitude of the node, for the initial conditions that entail maximal variations of the orbit inclination. The plot, obtained by integration of the semi-analytical model, demonstrates that inclination locking persists.

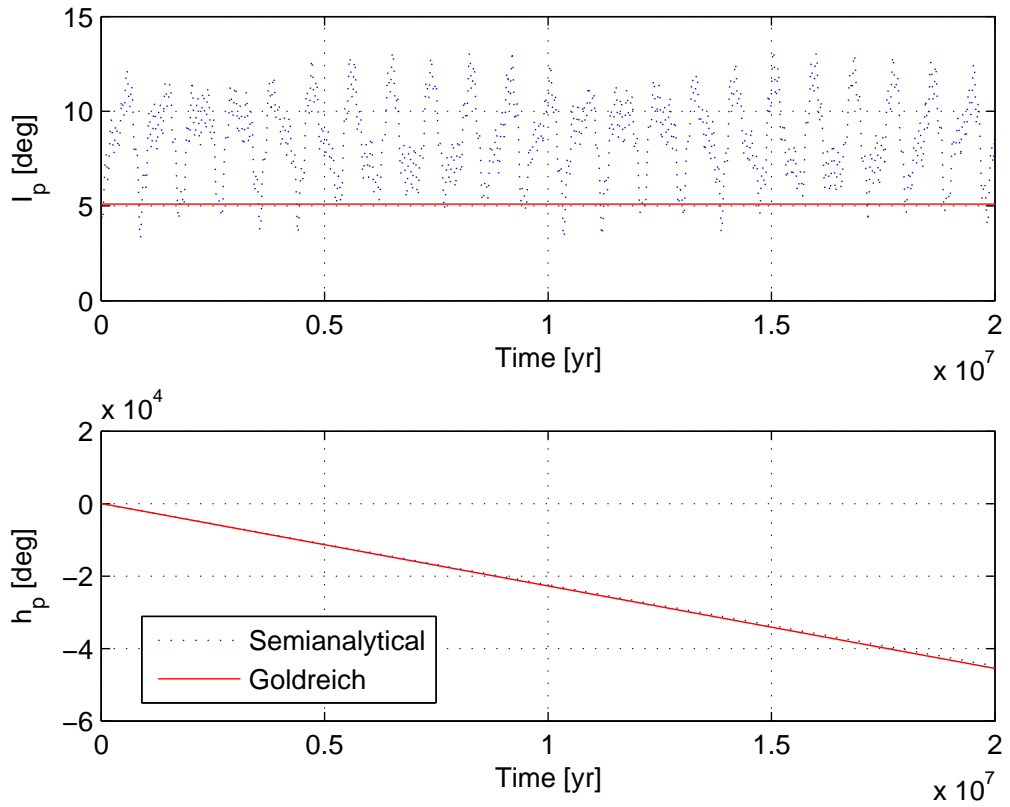


Figure 8: Preparation to comparison of the semianalytical model to Goldreich's model. In Goldreich's model, the Martian equator is assumed to precess uniformly, while the semianalytical model takes into account (via Colombo's equation) variations of the equinoctial precession.

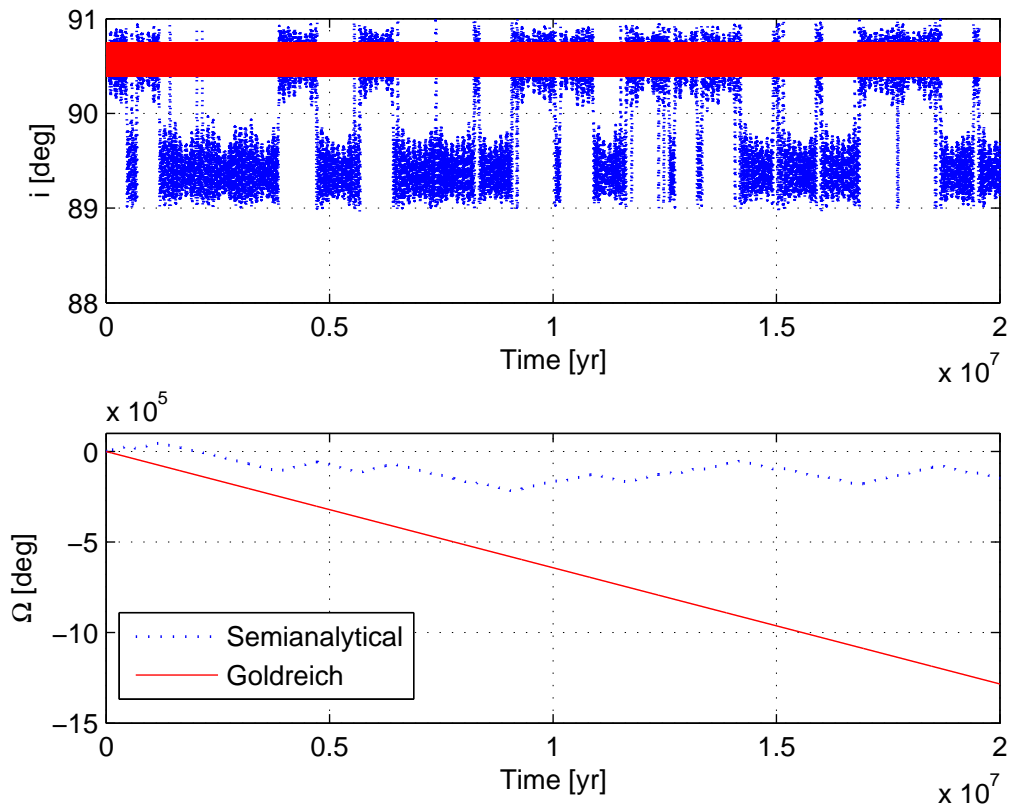


Figure 9: Comparison of the semi-analytical model to Goldreich's model. Deimos' inclination in Goldreich's model remains tightly locked, while the semianalytical model reveals much larger variations of the satellite's inclination.